ARCHIVES OF ELECTRICAL ENGINEERING VOL. 70(4), pp. 943–958 (2021)

DOI 10.24425/aee.2021.138271

The effect of closed loop control on diagnostic indices in different faults of squirrel cage induction motor

NOURELHOUDA BOUABID, MOHAMED-AMINE MOUSSA, YASSINE MAOUCHE, ABDELMALEK KHEZZAR

Departement d'electrotechnique, Laboratoire d'electrotechnique de Constantine
Universite Constantine 1, 25000 Constantine, Algeria
e-mail: nourelhouda.bouabid@lec-umc.org

(Received: 14.04.2021, revised: 19.06.2021)

Abstract: The aim of this work is to study the influence of closed loop control on diagnostic indices of both broken bar and mixed air-gap eccentricity fault indices of the squirrel cage induction motor drive. The present work is focused on the direct stator current i_{sd} signal analysis, which is independent of torque load when the induction motor is controlled by an indirect control field. The fault signatures are on the line extracted from the direct stator current signal using the discrete Fourier transformation (DFT). The formula of the measured direct stator current at both conditions is determined by the transfer function of the current loop. The obtained results show that the current loop corresponds to a low pass filter and can reduce the magnitude of diagnostic indicators which lead to wrong evaluation of the fault. Simulation and experiments were carried out in order to confirm the theoretical analysis.

Key words: closed loop control, discrete Fourier transformation, fault diagnostic, indirect filed control, rotor mechanical faults, squirrel cage induction motor

1. Introduction

The induction motor is the most widely used motor in industrial applications, due to its low cost, good performance, and excellent reliability [1–4]. Although the induction machine is known to be robust, however, it can sometimes have different types of faults. These latter induce failures leading to unscheduled shutdowns, production losses, costly repairs and can have serious consequences for the safety of people, equipment and the environment. It is therefore imperative to implement adequate monitoring systems aimed at detecting faults early.

In general, the failure of an electric machine can be classified as being electrical or mechanical depending on the root cause of the failure. Ref. [5] describes the structure of failures in electrical

machines. With the increasing dependence on electrical devices the monitoring of the condition of electrical machines is becoming very important to detect faults at an early stage [5, 6]. In [6], in areal experiment, there is no static eccentricity or dynamic eccentricity, there is the sum of two eccentricities, which means the existence of a mixed eccentricity.

The motor current signature analysis (MCSA) is the most used method to detect faults when the induction motor is fed directly from an isolated electrical grid [7–13]. The MCSA is the most popular method of online motor diagnosis for detecting motor faults such as broken bars, mixed eccentricity, or stator winding faults as presented in [14]. In [15] and [16] the authors presented the relation between the fluctuation amplitude of the fault level and mechanical load. In [17] and [18] the authors presented the problem appearing in the closed control when the induction motor was supplied by an inverter. The problem is the appearance of the undesirable additional harmonic components appearing in the current spectrum of the stator due to the switching process. This induces the difficulty of distinguishing between the presence and the absence of rotor cage faults. The influence of the closed current loop on the fault signatures of direct stator and quadrature currents has been presented in [19–21]. The utilized control data is available as direct stator currents and in quadrature to extract a correct fault index. In [22], the authors studied the influence of the closed loop on the diagnostics of faults in induction motors. The direct stator current is used because it is the most effective diagnostic index. Its amplitude is independent of the operating conditions and depends only on the fault level of the motor.

Diagnostics of broken rotor bar faults in an induction machine is studied in [23]. Utilized techniques are based on the vector quantization method (k-means), using a motor current signal analysis (MCSA) for the detection and classification, as well as the FFT approach for identification of the predominant frequency components.

Different methods to detect broken rotor bar faults in an induction motor are presented in [24–27].

The eccentricity of the machine is defined as an asymmetry in the air gap between the stator and the rotor, the nonhomogeneous distribution of the currents in the rotor and the imbalance of the stator currents. The imbalance of forces on the bars generates a non-constant overall torque. In [28] presented the types of eccentricity and its causes. In the case of static eccentricity, it is a constant pull in one direction. The minimum thickness of the air gap is fixed in space due to the ovality of the internal part of the stator or by the incorrect positioning of the rotor or stator during the construction phase. In the dynamic eccentricity type, the minimum thickness of the air gap rotates with the rotor (the centre of the rotor is not in its centre of rotation), due to the bending of the rotor shaft, the wear or misalignment of bearings, mechanical resonance at critical speed.

The interturn short-circuit is classified as an electrical fault. In [29–31] presented different methods to detect short-circuit faults in an induction motor.

Due to the flow of high currents in the remaining healthy phases during the existence of an open-circuit fault, the machine will be subjected to dangerously imbalanced voltages and overheating. In [32] proposed a strategy for diagnosing the open circuit fault, based on the comparison between the current signals of faulty and healthy currents of an induction motor model.

In [33], a bearing damage index (BDI) is proposed to detect the defective bearing.

There is no reference work that allows an analytical development of direct stator current when taking into account the effect of the presence of the fault signatures. In addition, no mention of

work suggested a way to overcome the effect of the current control loop. The object of this work is to deal with the analytical development of the effect of the current loop on the fault signatures. The current loop transfer function is utilized to obtain the attenuated formula of fault signatures. To extract the magnitude of fault indexes, we use the discrete Fourier transform.

This work is organised as follows: The mathematical model of the induction motor for fault conditions is presented in Section 2. The mathematical model of the induction motor for indirect field-oriented control is defined in Section 3. The impact of the closed loop on the direct stator current fault signatures is included in Section 4. The discrete Fourier transformation method is utilized in Section 5. Section 6 shows the simulation and experimental results and the conclusions are drawn in Section 7.

2. Mathematical model of the induction motor for fault condition

The squirrel-cage induction machine has three identical and symmetrical stator windings. Each of these windings is treated as a separate winding. The squirrel cage rotor consists of n_b bars. These bars are considered to be symmetrically spaced loops.

The electrical equations of the motor are as follows:

$$[v_s] = [R_s][i_s] + \frac{\mathrm{d}}{\mathrm{d}t}[\phi_s] + [v_n], \tag{1}$$

$$\begin{bmatrix} [v_r] \\ v_e \end{bmatrix} = \begin{bmatrix} [R_r] & \cdots & \dfrac{R_e}{n_b} \\ \vdots & \ddots & \vdots \\ \dfrac{R_e}{n_b} & \cdots & R_e \end{bmatrix} \begin{bmatrix} [i_r] \\ i_e \end{bmatrix} + \frac{\mathrm{d}}{\mathrm{d}t}[\phi_r], \tag{2}$$

$$[\phi_s] = [L_s][i_s] + [M_{sr}][i_r], \tag{3}$$

$$\begin{bmatrix} [\phi_r] \\ \phi_e \end{bmatrix} = \begin{bmatrix} [L_r] & \cdots & \dfrac{L_e}{n_b} \\ \vdots & \ddots & \vdots \\ \dfrac{L_e}{n_b} & \cdots & L_e \end{bmatrix} \begin{bmatrix} [i_r] \\ i_e \end{bmatrix} + \begin{bmatrix} [M_{rs}][i_s] \\ 0 \end{bmatrix}, \tag{4}$$

where:

$$[v_s] = \begin{bmatrix} v_{sa} & v_{sb} & v_{sc} \end{bmatrix}^t,$$
$$[i_s] = \begin{bmatrix} i_{sa} & i_{sb} & i_{sc} \end{bmatrix}^t$$

and

$$[\psi_s] = \begin{bmatrix} \psi_{sa} & \psi_{sb} & \psi_{sc} \end{bmatrix}^t.$$
$$[v_r] = \begin{bmatrix} v_{r1} & \cdots & v_{rn_b} \end{bmatrix}^t,$$
$$[i_r] = \begin{bmatrix} i_{r1} & \cdots & i_{rn_b} \end{bmatrix}^t$$

and

$$[\psi_r] = \begin{bmatrix} \psi_{r1} & \cdots & \psi_{rn_b} \end{bmatrix}^t$$

are the rotor voltages, current and flux linkage vectors, respectively, with a dimension of $(1 \times n_b)$, where n_b is number of rotor bars, and v_n is line neutral voltage.

The mutual inductance is given by the following equation:

$$M_{sqirk}(\theta) = \sum_{h=1}^{\infty} M_{sr}^h \cos\left(h\left(\theta + ka - (q-1)\frac{2\pi}{3} - \varphi_0\right)\right), \tag{5}$$

where:

$$M_{sr}^h = \frac{\mu_0 r L}{g_0} \frac{N_t}{\pi p^2} \frac{k_{wh}}{h^2} \sin\left(h\frac{a}{2}\right).$$

L is the length of stack, r is the average radius of the air gap, g_0 is the air gap function and N_t is the number of turns. K_{wh} is the winding factor and p is number of pole pairs. $a = p(2\pi/nb)$ is the electrical angle of a rotor loop. φ_0 is the initial phase angle. $q = 1,\ 2,\ 3$ is the q-th stator phase. h is the order of space harmonics resulting from the mutual inductance linkage. θ is electrical angular position.

3. The mathematical model of the induction motor for indirect field-oriented control

The principle of the field-oriented control (FOC) method is to operate the induction motor as a DC motor with independent control of torque and flux control, based on torque decoupling technique and the flux control method for AC motors. The indirect flux-orientation method is based on the reverse dynamics of the motor's flux model. Thanks to the simplicity of its implementation the rotor flux orientation scheme is the most commonly used. The flux position is estimated by the motor model in which the rotor flux is orientated by the d-axis, rendering the part of the q-axis equivalent to zero.

The usual assumptions to use the indirect field-oriented control approach is that the effect of saturation is neglected. An induction motor machine model was established using the synchronously rotating reference of stators and rotors. Which is presented by the following equations:

$$\begin{cases} v_{sd} = R_s I_{sd} + \dfrac{\mathrm{d}\psi_{sd}}{\mathrm{d}t} - \omega_s \psi_{sq} \\ v_{sq} = R_s I_{sq} + \dfrac{\mathrm{d}\psi_{sq}}{\mathrm{d}t} + \omega_s \psi_{sd} \\ v_{rd} = 0 = R_r I_{rd} + \dfrac{\mathrm{d}\psi_{rd}}{\mathrm{d}t} - \omega_r \psi_{rq} \\ v_{rq} = 0 = R_r I_{rq} + \dfrac{\mathrm{d}\psi_{rq}}{\mathrm{d}t} + \omega_r \psi_{rd} \end{cases}, \tag{6}$$

where:

$$\begin{cases} \psi_{sd} = L_s I_{sd} + L_m I_{rd} \\ \psi_{sq} = L_s I_{sq} + L_m I_{rq} \\ \psi_{rd} = L_r I_{rd} + L_m I_{sd} \\ \psi_{rq} = L_r I_{rq} + L_m I_{sq} \end{cases}. \tag{7}$$

The equation of electromagnetic torque is defined by:

$$\Gamma_e = p\frac{L_m}{L_r}\left(\psi_{rd} I_{sd} - \psi_{rq} I_{rd}\right). \tag{8}$$

To render the machine operate like a direct current machine with separated excitation, we use the following formulae:

$$\begin{cases} \psi_{rq} = 0 & \dfrac{\mathrm{d}\psi_{rq}}{\mathrm{d}t} = 0 \\ \psi_{rd} = \psi_r \end{cases}. \tag{9}$$

By putting Eq. (9) in (6) and (8), we find:

$$\begin{cases} v_{sd} = R_s I_{sd} + L_s \sigma s I_{sd} - \omega_s \sigma L_s I_{sq} \\ v_{sq} = R_s I_{sq} + L_s \sigma s I_{sq} + \omega_s \sigma L_s I_{sd} + \omega_s \dfrac{M}{L_r}\psi_r \\ \tau_r s\psi_r + \psi_r = M_{sr} I_{sd}^* \qquad \omega_s - \omega = \dfrac{I_{sq}}{\tau_r I_{sd}} \qquad \Gamma_e = p\dfrac{M_{sr}}{L_r}\psi_r I_{sq} \end{cases}, \tag{10}$$

where: v_{sd}, v_{sq}, I_{sd}, I_{sq}, ψ_{sd}, ψ_{sq} are the direct and quadrature stator voltages, current and flux, respectively. v_{rd}, v_{rq}, I_{rd}, I_{rq}, ψ_{rd}, ψ_{rq} are the direct and quadrature rotor voltages, current and flux, respectively. R_s, R_r stator and rotor resistance, L_s, L_r, L_m are the self-inductance of stator and rotor, Magnetizing inductances respectively. Γ_e is electromagnetic torque. $s = \dfrac{\mathrm{d}}{\mathrm{d}t}$ represents the Laplace operator. $\tau_r = \dfrac{L_r}{R_r}$ and $\sigma = 1 - \dfrac{M_{sr}^2}{L_S L_r}$.

4. The impact of a closed loop on the direct stator current fault signatures

The induction motor fault like a broken bar or mixed eccentricity faults, can hold many harmonic components in measured currents, its spectrum has high amplitudes next to the fundamental components relative to other fault signatures in the high frequency.

4.1. Eccentricity fault

The eccentricity of the machine is defined as an asymmetry in the air gap between the stator and rotor, the non-homogeneous distribution of currents in the rotor and the unbalance of the stator currents. The imbalance of the forces on the bars generates a non-constant overall torque.

Rotor eccentricity in induction motors takes 3 types: The minimum air gap is spatially fixed: this type is named eccentricity static. In eccentricity dynamic, the minimum air gap thickness

rotates with the rotor. In practice, there is no static eccentricity or dynamic eccentricity, there is the sum of the two eccentricities, the mixed eccentricity. Its frequency in the stator current is set by:

$$f_{ecc} = f_s \pm f_m = \left| f_s \pm k \left(\frac{1-s}{p} f_s \right) \right|_{k=1,2,3,\ldots},$$

where f_s is the frequency of fundamental harmonic.

4.2. Rotor broken bars fault

Among the most studied faults, the breakage of rotor bars of an induction motors, is undoubtedly one of the most common. Failure of a rotor bar or short circuit ring segment can be caused by several factors, often independent of each other. The frequencies of spectral components in the stator current are as follows:

$$f_{\text{rotor}} = |(1 \pm 2ks) f_s|_{k=1,2,3,\ldots}.$$

4.3. The direct stator current fault signatures

The equations of the stator current in the case of the defect are as follows:

$$\begin{bmatrix} i_{sa} \\ i_{sb} \\ i_{sc} \end{bmatrix} = \begin{bmatrix} I_m \cos(\omega_s t - \phi_0) + I_{md} \cos(\omega_f t - \phi_f) \\ I_m \cos\left(\omega_s t - \phi_0 - \dfrac{2\pi}{3}\right) + I_{md} \cos\left(\omega_f t - \phi_f - \dfrac{2\pi}{3}\right) \\ I_m \cos\left(\omega_s t - \phi_0 + \dfrac{2\pi}{3}\right) + I_{md} \cos\left(\omega_f t - \phi_f + \dfrac{2\pi}{3}\right) \end{bmatrix}. \tag{11}$$

The following model uses the Concordia transformation, based on the transformation of three-phase currents, from *abc* coordinates to $\alpha\beta$ coordinates, which is given by:

$$\begin{bmatrix} i_{s\alpha} \\ i_{s\beta} \end{bmatrix} = \sqrt{\frac{2}{3}} \begin{bmatrix} 1 & -\dfrac{1}{2} & -\dfrac{1}{2} \\ 0 & \dfrac{\sqrt{3}}{2} & -\dfrac{\sqrt{3}}{2} \end{bmatrix} \begin{bmatrix} i_{sa} \\ i_{sb} \\ i_{sc} \end{bmatrix}. \tag{12}$$

By putting Eq. (11) into (12), we find:

$$\begin{cases} i_{s\alpha} = \dfrac{\sqrt{3}}{2} I_m \cos(\omega_s t - \phi_0) + \dfrac{\sqrt{3}}{2} I_{md} \cos\left(\omega_f t - \phi_f\right) \\ i_{s\beta} = \dfrac{\sqrt{3}}{2} I_m \sin(\omega_s t - \phi_0) + \dfrac{\sqrt{3}}{2} I_{md} \sin\left(\omega_f t - \phi_f\right) \end{cases}. \tag{13}$$

To transform the currents to a synchronous reference, a rotational transformation $[R(\theta s)]$ is used, which can be written as follows:

$$[R(\theta_s)] = \begin{bmatrix} \cos(\theta_s) & \sin(\theta_s) \\ -\sin(\theta_s) & \cos(\theta_s) \end{bmatrix}. \tag{14}$$

By using the rotational transformation, we get:

$$\begin{cases} i_{sd} = \dfrac{\sqrt{3}}{2} I_m \cos(\phi_0) + \dfrac{\sqrt{3}}{2} I_{md} \cos\left((\omega_s - \omega_f)t - \phi_f\right) \\ i_{sq} = \dfrac{\sqrt{3}}{2} I_m \sin(\phi_0) + \dfrac{\sqrt{3}}{2} I_{md} \sin\left((\omega_s - \omega_f)t - \phi_f\right) \end{cases}, \tag{15}$$

where: ω_s is the fundamental pulsation of the stator current, and ω_f is pulsation of the harmonic component. ϕ_0, ϕ_f, θ_s are initial phase angle of the stator current, pulsation of the harmonic component, stator angular position, respectively.

I_m, I_{md} are the maximum value of the fundamental component stator current, amplitude of the harmonic component of the voltage and current systems, respectively.

Based on these equations it can be noticed that the current component contains two parts, a continuous part and an alternative part, such pulsation of the alternative part is $\omega_s - \omega_f$, so:

$$\begin{cases} i_{sd} = \overline{I}_{sd} + \widetilde{I}_{sd} \\ i_{sq} = \overline{I}_{sq} + \widetilde{I}_{sq} \end{cases}. \tag{16}$$

As stated earlier, direct current is suitable for the monitoring of three-phase induction motor faults, because it is not dependent on the mechanical load variation.

The block diagram of the direct stator current I_{sd} control loop is shown in Fig. 1.

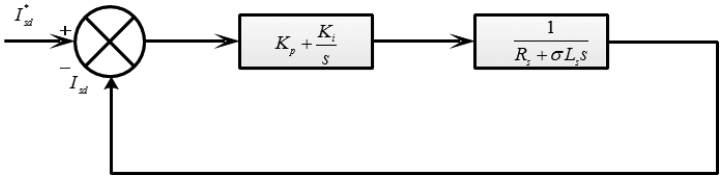

Fig. 1. The block diagram of direct stator current I_{sd} control loop

In order to study the effect of the closed loop on the amplitude of the direct stator current under faulty conditions, the transfer function must be determined as follows:

$$H(s) = \frac{G_1(s)G_2(s)}{1 + G_1(s)G_2(s)}.$$

The first block presents the transfer function of a PI controller that can be written as follows:

$$G_1(s) = K_p + \frac{K_i}{s}.$$

The second block presents the transfer function of the controlled system, defined as follows:

$$G_2(s) = \frac{1}{R_S + \sigma L_S s}.$$

The transfer function of the direct stator current loop is given by:

$$H(s) = \frac{K_p s + K_i}{s^2 + 2\xi\omega_n s + \omega_n^2}. \tag{17}$$

It can be noticed that Eq. (17) acts as a transfer function of a low-pass filters, and passes a pulsation lower than $\sqrt{\dfrac{K_i}{\sigma L_s}}$.

The transfer function of the low-pass filter is as follows:

$$H(s) = \frac{K\omega_n^2}{s^2 + 2\xi\omega_n s + \omega_n^2}. \tag{18}$$

The temporal filtered output response of the precedent equation presents the measured direct stator current, which takes the following form:

$$\begin{aligned} i_{sd}(t) = {} & \frac{\sqrt{3}}{2} I_m \cos(\phi_0) \times \left(1 + e^{-\xi\omega_n t}\sqrt{\frac{1}{1-\xi^2}}\cos\left(\omega_n\sqrt{1-\xi^2}t - \phi\right)\right) + \\ & + K\omega_n^2 \frac{\sqrt{3}}{2} I_{md} \times a_1 \sin\left((\omega_s - \omega_f)t + \phi_1\right) + a_2 e^{-\xi\omega_n t}\cos\left(\omega_n\sqrt{1-\xi^2}t - \phi_1\right), \end{aligned} \tag{19}$$

where:

$$a_1 = \frac{1}{\omega_s - \omega_f}\sqrt{\frac{1}{(\omega_s - \omega_f)^2 + \dfrac{\omega_n^2}{(\omega_s - \omega_f)^2} + 2\omega_n^2(2\xi^2 - 1)}},$$

$$a_2 = (\omega_s - \omega_f)^2 \sqrt{\frac{\left(-\xi - \dfrac{-\xi\omega_n^2}{(\omega_s - \omega_f)^2}\right)^2 \left(\dfrac{1}{(1-\xi^2)^2}\right) + \left(1 + \dfrac{\omega_n^2}{(\omega_s - \omega_f)^2}\right)^2}{\left[\left(2\xi^2\omega_n^2 - \omega_n^2 + (\omega_s - \omega_f)^2\right)^2 + \left(2\xi\omega_n^2\sqrt{1-\xi^2}\right)^2\right]^2}}.$$

It can be noticed that the equation which is presented as Eq. (19) consists of two transient responses: $\overline{I}_{sd}$, $\widetilde{I}_{sd}$.

$$\begin{aligned} \overline{I}_{sd} = {} & \frac{\sqrt{3}}{2} I_m \cos(\phi_0) \times \left(1 + e^{-\xi\omega_n t}\sqrt{\frac{1}{1-\xi^2}}\cos\left(\omega_n\sqrt{1-\xi^2}t - \phi\right)\right) + \\ & + K\omega_n^2 \frac{\sqrt{3}}{2} I_{md} a_2 e^{-\xi\omega_n t}\cos\left(\omega_n\sqrt{1-\xi^2}t - \phi_1\right). \end{aligned} \tag{20}$$

Equation (20), this component defines the continuous harmonic.

$$\widetilde{I}_{sd} = K\omega_n^2 \frac{\sqrt{3}}{2} I_{md} a_1 \sin\left((\omega_s - \omega_f)t + \phi_1\right). \tag{21}$$

Equation (21), this response presents the harmonic component of the fault signature.

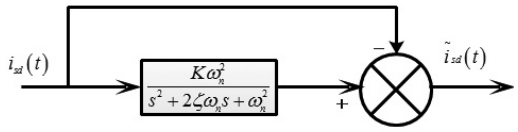

Fig. 2. The block diagram of the fault signature extraction from the direct stator current I_{sd} control loop

The block diagram of the fault signature extraction from the musearude direct stator current *Isd* control loop is shown in Fig. 2.

In order to get the alternative part of the fault signature, the subtraction of the continuous part was used, as presented in Fig. 2. It can be written as follows:

$$\widetilde{I}_{sd} = I'_{md}\sin(2\pi f_f t + \phi_1), \tag{22}$$

where:

$$I'_{md} = K\omega_n^2\frac{\sqrt{3}}{2}I_{md}a_1\,, \qquad f_f = \frac{\omega_s - \omega_f}{2\pi}\,.$$

ω_n, ξ, f_f, I'_{md} are the cut-off pulsation, the damping ration, frequency of the fault signature, and the amplitude of the attenuated fault signature, respectively.

5. Discrete Fourier transformation method

To see the impact of a PI controller on the magnitude of the attenuated fault signature, the discrete Fourier transform (DFT) was used (see Fig. 3).

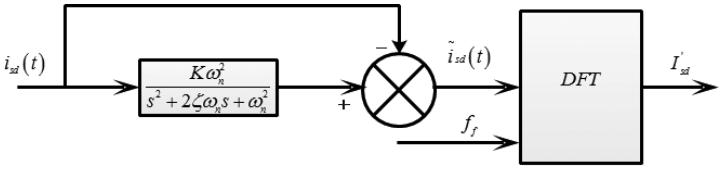

Fig. 3. The discrete Fourier transformation of the fault signature

The function that determines the signal as a function of frequency is presented by Eq. (23)

$$X(W) = \sum_{n=0}^{N-1} X(nT_e)e^{-j\omega_n nT_e}, \tag{23}$$

where:

$$W = K\frac{\omega_e}{N}\,, \qquad \omega_e = 2\pi F_e\,, \qquad \Delta f = \frac{F_e}{N}\,.$$

Δf, N, F_e, T_e are frequency step, number of points, sampling frequency and frequency, respectively.

$$X\left(K\frac{\omega_e}{N}\right) = \sum_{n=0}^{N-1} X(nT_e)e^{-jK\frac{\omega_e}{N}nT_e}. \tag{24}$$

The formula of the fault signature $\widetilde{I}_{sd}$ in terms of frequency is as follows:

$$A_{\widetilde{I}_{sd}} = \sum_{n=0}^{N-1} \widetilde{I}_{sd}(nT_e)e^{-j\omega_n nT_e}. \tag{25}$$

By replacing Eq. (22) with Eq. (25), we obtain the following:

$$A_{\widetilde{I}_{sd}} = 2\sum_{n=0}^{N-1} \frac{I_{md}}{2} \sin(2\pi nT_e(k\Delta f \pm f_f) \pm \phi_1) - j\cos(2\pi nT_e(k\Delta f \pm f_f) \pm \phi_1). \tag{26}$$

6. Simulation and experimental results

To validate the theoretical analysis, the simulation and experiment are described in this section. The parameters of the simulated induction motor are presented in Table 1.

Table 1. Specification of simulated three-phase induction motor

Specification	**IM**
Rated power	1.1 KW
Stator slots	24
Of rotor bars	22
Poles	2 P

Suppose the direct stator current takes the form below:

$$I_{sd} = 1\cos(2\pi f_s t + \phi_0) + 0.4\cos\left(2\pi f_f t + \phi_1\right). \tag{27}$$

Table 2, shows the specifications of I_{sd}.

Table 2. Specification of direct stator current

Specification	$\boldsymbol{I_{sd}}$
f_s	40 Hz
f_f	6 Hz
ω_n	981 rad/s
ξ	0.7

The measured direct stator current given by Eq. (19) is illustrated in Fig. 4. As shown in Fig. 4, the measured direct stator current consists of two parts to respond: one presents a continuous part and the second defines the alternative part in case of a broken bar fault. It can be noticed that the supposed value of the continuous part magnitude is the same in the simulation; on the other hand, in the alternative part the assumed value of the magnitude is decreased. This result can be confirmed by Eqs. (19) and (25).

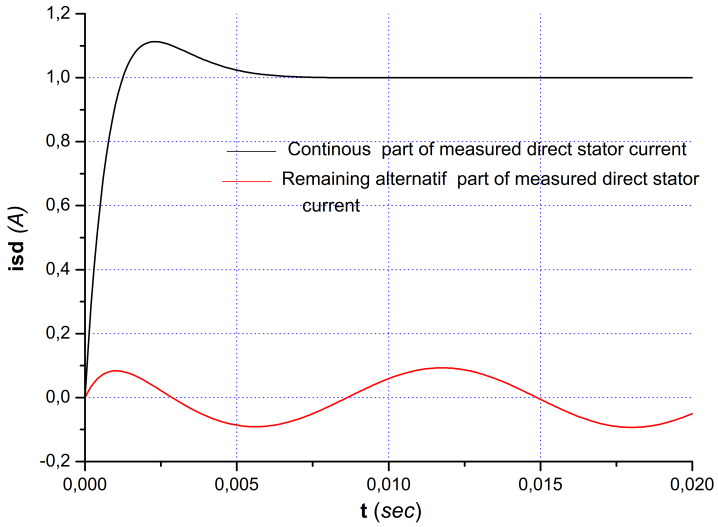

Fig. 4. Measured direct stator current in case of broken bar fault

The magnitude of the fault signature at different fault frequencies is shown in Figs. 5(a) and (b). It is extracted by using a DFT algorithm.

Table 3 shows the magnitude values of the i_{sd} current component in the closed loop system and its fault signature percentage under a rotor broken bar, and mixed eccentricity respectively.

Table 3. Magnitude percentage of the fault signature in the case of broken bar fault and mixed eccentricity fault

Broken bar fault				**Mixed eccentricity fault**			
Fault frequency	Magnitude of fault signature	Magnitude of fault signature (%)	Magnitude of fault signature decrease percentage	Fault frequency	Magnitude of fault signature	Magnitude of fault signature (%)	Magnitude of fault signature decrease percentage
6.419	0.00219	0.5475	99.4525%	9.60	0.00589	1.4743	98.5257%
6.492	0.00224	0.5600	99.4400%	14.40	0.00969	2.4257	97.5743%
6.565	0.00239	0.5975	99.4025%	19.20	0.01381	3.4513	96.5487%
6.637	0.00278	0.6950	99.305%	24.00	0.01835	4.5886	95.4114%
6.71	0.00329	0.8225	99.1775%	33.60	0.02891	7.2289	92.7711%
/	/	/	/	38.40	0.03501	8.7529	91.2471%

Real magnitude's simulation value is 0.4 A. It can be seen in the second column of Table 3 that the significant decrease in the fault signature's magnitude was compared to the real value. When using the control loop, the amplitude decreases greatly, which is expressed as a percentage in the

fourth column of Table 3 (magnitude of fault signature decreased percentage). It means that the closed-loop causes the minimization of the fault magnitude, due to the existence of a regulator. The regulator forces the controlled variable to the reference value. This operation has an influence on the diagnosis, which causes difficulty in detecting the fault.

The simulation results of the measured direct stator current are shown in Fig. 6(a) healthy, (b), (c) and (d) with broken bar faults at various frequencies. These results have validated the preceding computation. Regardless of the frequency change, it can be noticed that the amplitude values of the fault signature that are shown in Fig. 6(b), (c) and (d) are very close to the healthy condition magnitude values shown in Fig. 6(a). This is due to the closed loop effect.

The experimental setup is presented in Fig. 5. This setup, which contains of the specifications of the three-phase induction motor, is as follows (Table 4):

Fig. 5. Test bench

Table 4. Specification of experimented three-phase induction motor

Specification	**IM**
Rated power	1.1 KW
Stator slots	24
Of rotor bars	22
Poles	2P
Voltages	400 V
Frequency	50 Hz

The motor is powered by a three-phase inverter (SEMIKRON). The digital signal processor board (dspace 1104) is used for monitoring. In order to provide the DC link voltage to the VSC, DC power supply is utilized. A magnetic powder brake is mechanically coupled to the induction motor.

The experimental results are shown in Fig. 6 and Fig. 7(a) healthy, (b), (c) and (d) with a broken bar fault and eccentricity fault at different frequencies respectively. It is observed that

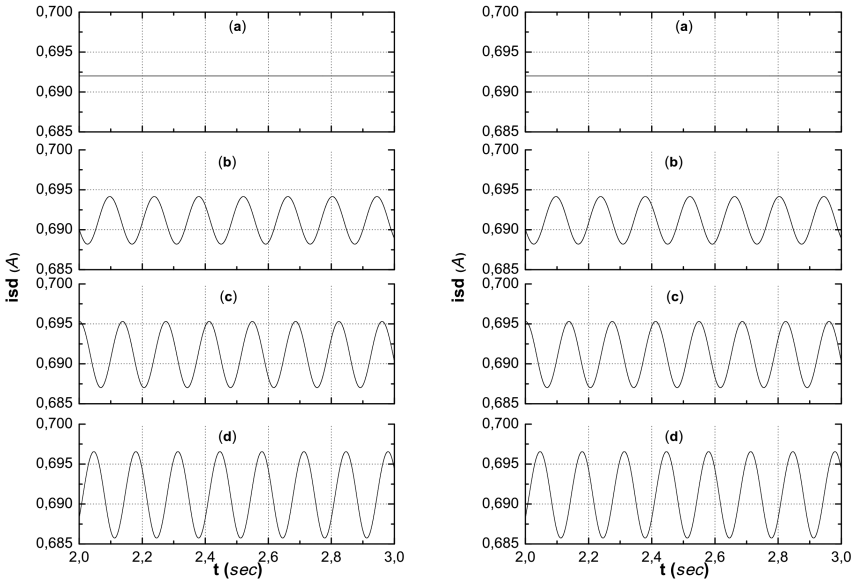

(A) (B)

Fig. 6. (A) simulation results, (B) experimental results of the direct stator current measured: (a) healthy; (b), (c) and (d) in the case of broken bar fault at various frequencies

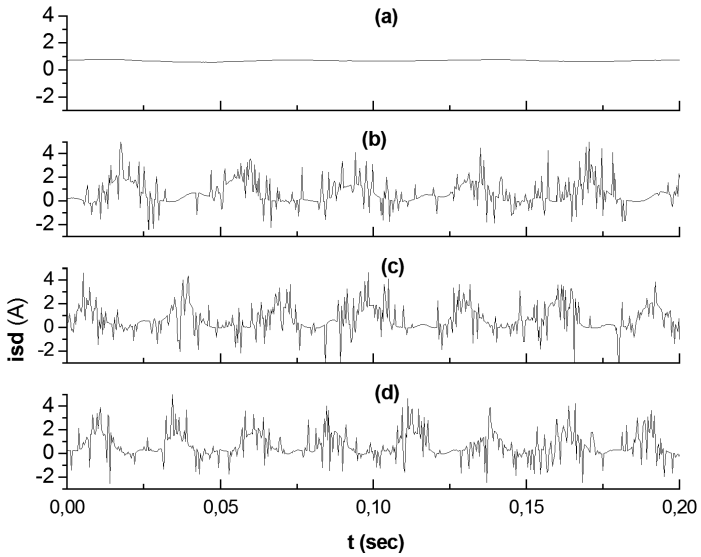

Fig. 7. Experimental results of the direct stator current measured: (a) healthy; (b), (c) and (d) in the case of eccenricity fault at various frequencies

in the case of broken bar and eccentricity faults, magnitude values are very close to those given by healthy conditions. Equation (25) and simulation results corroborate the effect of closed loop control on diagnostic indices.

7. Conclusions

This paper has investigated the effect of closed loop control on the magnitude of the direct stator current measured in different faults (broken bar and mixed eccentricity). The basis of this study was utilizing the transfer function of the direct stator current control loop to deduce the expanded formula at both conditions (healthy and fault conditions). This study allows one to find the effect of closed loop control on the magnitude of the direct stator current under faulty condition formulation. In addition, the research shows the existence of a regulator minimizes the amplitude values of the fault signature. It has been shown that when using the control loop, the magnitude of the direct stator current decreases greatly. The discrete Fourier transform (DFT) is used to extract the magnitude of the fault signature from the direct stator current signal. The theoretical analysis and the simulation results were validated by the experimental results.

References

[1] Hou Z., Huang J., Liu H., Ye M., Liu Z., Yang J., *Diagnosis of broken rotor bar fault in open-and closed loop controlled wye-connected induction motors using zero sequence voltage*, IET Electric Power Applications, vol. 11, no. 7, pp. 1214–1223 (2017), DOI: 10.1049/iet-epa.2016.0505.

[2] Blodt M., Granjon P., Raison B., Rostaing G., *Models for bearing damage detection in induction motors using stator current monitoring*, IEEE transactions on industrial electronics, vol. 55, no. 4, pp. 1813–1822 (2008), DOI: 10.1109/TIE.2008.917108.

[3] Jung J.H., Lee J.J., Kwon B.H., *Online diagnosis of induction motors using MCSA*, IEEE Transactions on Industrial Electronics, vol. 53, no. 6, pp. 1842–1852 (2006), DOI: 10.1109/TIE.2006.885131.

[4] Song X., Hu J., Zhu H., Zhang J., *A bearing outer raceway fault detection method in induction motors based on instantaneous frequency of the stator current*, IEEJ Transactions on Electrical and Electronic Engineering, vol. 13, no. 3, pp. 510–516 (2018), DOI: 10.1002/tee.22595.

[5] Basak D., Tiwari A., Das S.P., *Fault diagnosis and condition monitoring of electrical machines – A Review*, In 2006, IEEE International Conference on Industrial Technology, pp. 3061–3066 (2006), DOI: 10.1109/ICIT.2006.372719.

[6] Huang X., Habetler T.G., *Detection of mixed air gap eccentricity in closed-loop drive-connected induction motors*, In 4th IEEE International Symposium on Diagnostics for Electric Machines, Power Electronics and Drives, 2003, SDEMPED 2003, pp. 312–316 (2003), DOI: 10.1109/DEMPED.2003.1234592.

[7] Nandi S., Toliyat H.A., Li X., *Condition monitoring and fault diagnosis of electrical motors – A review*, IEEE Transactions on Energy Conversion, vol. 20, no. 4, pp. 719–729 (2005), DOI: 10.1109/TEC.2005.847955.

[8] Henao H., Razik H., Capolino G.A. *Analytical approach of the stator current frequency harmonics computation for detection of induction machine rotor faults*, IEEE Transactions on Industry Applications, vol. 41, no. 3, pp. 801–807 (2005), DOI: 10.1109/TIA.2005.847320.

[9] Blodt M., Regnier J., Faucher J., *Distinguishing load torque oscillations and eccentricity faults in induction motors using stator current Wigner distributions*, IEEE Transactions on Industry Applications, vol. 45, no. 6, pp. 1991–2000 (2009), DOI: 10.1109/TIA.2009.2031888.

[10] Maouche Y., Boussaid A., Boucherma M., Khezzar A., *Analytical study of pulsating torque and harmonic components in rotor current of six-phase induction motor under healthy and faulty conditions*, In 2013, 9th IEEE International Symposium on Diagnostics for Electric Machines, Power Electronics and Drives (SDEMPED), pp. 295–301 (2013), DOI: 10.1109/DEMPED.2013.6645731.

[11] Maouche Y., Oumaamar M.E.K., Boucherma M., Khezzar A., *Instantaneous power spectrum analysis for broken bar fault detection in inverter-fed six-phase squirrel cage induction motor*, International Journal of Electrical Power and Energy Systems, vol. 62, pp. 110–117 (2014), DOI: 10.1016/j.ijepes.2014.04.030.

[12] Maouche Y., Boussaid A., Boucherma M., Khezzar A., *Modeling and simulation of stator turn faults. Detection based on stator circular current and neutral voltage*, In 2013, 9th IEEE International Symposium on Diagnostics for Electric Machines, Power Electronics and Drives (SDEMPED), pp. 263–268 (2013), DOI: 10.1109/DEMPED.2013.6645726.

[13] Yacine M., *Contribution a l'etude de la machine asynchrone double etoile*, Université Mentouri Constantine (2015).

[14] Huang X., Habetler T.G., Harley R.G., *Analysis, simulation, and experiments of rotor eccentricity in closed-loop drive-connected induction motors*, In 2005, 5th IEEE International Symposium on Diagnostics for Electric Machines, Power Electronics and Drives, pp. 1–6 (2005), DOI: 10.1109/DEMPED.2005.4662518.

[15] Xu B., Sun L., Ren H., *A new criterion for the quantification of broken rotor bars in induction motors*, IEEE Transactions on Energy Conversion, vol. 25, no. 1, pp. 100–106 (2009), DOI: 10.1109/TEC.2009.2032626.

[16] Bossio G.R., De Angelo C.H., Bossio J.M., Pezzani C.M., Garcia G.O., *Separating broken rotor bars and load oscillations on IM fault diagnosis through the instantaneous active and reactive currents*, IEEE Transactions on Industrial Electronics, vol. 56, no. 11, pp. 4571–4580 (2009), DOI: 10.1109/TIE.2009.2024656.

[17] Kral C., Wieser R.S., Pirker F., Schagginger M., *Sequences of field-oriented control for the detection of faulty rotor bars in induction machines-the Vienna Monitoring Method*, IEEE Transactions on Industrial Electronics, vol. 47, no. 5, pp. 1042–1050 (2000), DOI: 10.1109/41.873212.

[18] Akin B., Orguner U., Toliyat H.A., Rayner M., *Low order PWM inverter harmonics contributions to the inverter-fed induction machine fault diagnosis*, IEEE Transactions on Industrial Electronics, vol. 55, no. 2, pp. 610–619 (2008), DOI: 10.1109/TIE.2007.911954.

[19] Cruz S.M., Stefani A., Filippetti F., Cardoso A.J.M., *A new model-based technique for the diagnosis of rotor faults in RFOC induction motor drives*, IEEE Transactions on Industrial Electronics, vol. 55, no. 12, pp. 4218–4228 (2008), DOI: 10.1109/TIE.2008.2003365.

[20] Bossio G.R., De Angelo C.H., Garcia G.O., Solsona J.A., Valla M.I., *Effects of rotor bar and end-ring faults over the signals of a position estimation strategy for induction motors*, IEEE transactions on industry applications, vol. 41, no. 4, pp. 1005–1012 (2005), DOI: 10.1109/TIA.2005.851038.

[21] Ellini A., Filippetti F., Franceschini G., Tassoni C., *Closed-loop control impact on the diagnosis of induction motors faults*, IEEE transactions on Industry Applications, vol. 36, no. 5, pp. 1318–1329 (2000), DOI: 10.1109/28.871280.

[22] Bellini A., Concari C., Franceschini G., Tassoni C., *Different procedures for the diagnosis of rotor fault in closed loop induction motors drives*, In 2007, IEEE International Electric Machines and Drives Conference, vol. 2, pp. 1427–1433 (2007), DOI: 10.1109/IEMDC.2007.383638.

[23] Ouachtouk I., El Hani S., Guedira S., Dahi K., *Detection and classification of broken rotor bars faults in induction machine using K-means classifier*, In 2016, International Conference on Electrical and Information Technologies (ICEIT), pp. 180–185 (2016), DOI: 10.1109/EITech.2016.7519586.

[24] Wu Y., An Q., *Online diagnosis of broken rotor bar fault of squirrel-cage induction motor using a magnetic field measuring coil*, IEEJ Transactions on Electrical and Electronic Engineering, vol. 15, no. 2, pp. 291–303 (2020), DOI: 10.1002/tee.23056.

[25] Nakamura H., Pandarakone S.E., Mizuno Y., *A novel approach for detecting broken rotor bar around rated rotating speed using frequency component and clustering*, IEEJ Transactions on Electrical and Electronic Engineering, vol. 11, pp. S116-S122 (2016), DOI: 10.1002/tee.22343.

[26] Hassan O.E., Amer M., Abdelsalam A.K., Williams B.W., *Induction motor broken rotor bar fault detection techniques based on fault signature analysis–a review*, IET Electric Power Applications, vol. 12, no. 7, pp. 895–907 (2018), DOI: 10.1049/iet-epa.2018.0054.

[27] Sousa K.M., da Costa I.B.V., Maciel E.S., Rocha J.E., Martelli C., da Silva J.C.C., *Broken bar fault detection in induction motor by using optical fiber strain sensors*, IEEE Sensors Journal, vol. 17, no. 12, pp. 3669–3676 (2017), DOI: 10.1109/jsen.2017.269596.

[28] Dorrell D.G., Thomson W.T., Roach S., *Analysis of airgap flux, current, and vibration signals as a function of the combination of static and dynamic airgap eccentricity in 3-phase induction motors*, IEEE Transactions on Industry applications, vol. 33, no. 1, pp. 24–34 (1997), DOI: 10.1109/28.567073.

[29] Rajamany G., Srinivasan S., *Neural Network Approach for Inter-turn Short-Circuit Detection in Induction Motor Stator Winding*, In Artificial Intelligence and Evolutionary Computations in Engineering Systems, Springer, Singapore, pp. 537–550 (2018), DOI: 10.1007/978-981-10-7868-2_52.

[30] Rajamany G., Srinivasan S., Rajamany K., Natarajan R.K., *Induction motor stator interturn short circuit fault detection in accordance with line current sequence components using artificial neural network*, Journal of Electrical and Computer Engineering (2019), DOI: 10.1155/2019/4825787.

[31] Rajamany G., Rajamany K., Natarajan R.K., *Negative Sequence Current Compensation for Induction Motor Stator Inter-Turn Short Circuit and Off-Diagonal Term in Sequence Impedance Matrix as Fault Indicator*, Journal of Electrical Engineering Technology, pp. 1–8 (2021), DOI: 10.1007/s42835-021-00730-8.

[32] Aswad R.A., Jassim B.M., *Open-circuit fault diagnosis in three-phase induction motor using model-based technique*. Archives of Electrical Engineering, vol. 69, no. 4 (2020), DOI: 10.24425/aee.2020.134632.

[33] Patel R.K., Giri V.K., *Condition monitoring of induction motor bearing based on bearing damage index*, Archives of Electrical Engineering, vol. 66, no. 1, pp. 105–119 (2017), DOI: 10.1515/aee-2017-0008.